

A new approach to resolving climate-cryosphere relations: Downscaling climate dynamics to glacier-scale mass and energy balance without statistical scale linking

Thomas Mölg¹ and Georg Kaser¹

Received 21 January 2011; revised 5 May 2011; accepted 12 May 2011; published 16 August 2011.

[1] We present a novel combination of methods to quantify the local mass response of mountain glaciers to large-scale circulation. Previously, such multiscale approaches bypassed the mesoscale processes of the mountain-induced atmospheric flow, by statistical transfer functions or subgrid parameterizations, and included simplified glacier mass balance (MB) models. Here we show, on the basis of Kilimanjaro (East Africa) as a test case, that a limited area atmospheric model (LAM) and a process-resolving MB model can be linked without statistical corrections at their interface. This is evident from robust energy and MB patterns at the glacier surface, regardless of whether the MB model is forced by (1) in situ meteorological measurements or (2) uncorrected output from the high-resolution LAM grid over the glacier area. The latter is achieved by multiple grid nesting in the land-atmosphere-ocean domain of the LAM. Since this setup resolves the mesoscale process space, we also show the potential to increase knowledge of how dynamical, thermodynamic, and microphysical phenomena of the mountain-induced flow affect glacier MB. All these results are encouraging for future research because they demonstrate that a dynamical system, which operates on very different space-time scales, can be quantified in a fully physical way, if dynamic meteorology and glaciology are exploited in a complementary sense. This will enhance the process understanding of forward problems (glacier response to climate forcing) and backward problems (climate signal extraction from past extents of mountain glaciers).

Citation: Mölg, T., and G. Kaser (2011), A new approach to resolving climate-cryosphere relations: Downscaling climate dynamics to glacier-scale mass and energy balance without statistical scale linking, *J. Geophys. Res.*, 116, D16101, doi:10.1029/2011JD015669.

1. Introduction and State of the Art

[2] Linking climate dynamics with models of glacier mass balance (MB) is crucial to obtaining an idea of how large-scale climate change affects glacier behavior locally or, in the inverse direction, of what historic glacier changes tell us about the climate of preinstrumental periods. Our research on Kilimanjaro has demonstrated the value of studies of mountain glaciers for improving the physical understanding of climate change and its dynamics across multiple space-time scales. This was revealed by studying small-scale energy and mass exchanges at the glacier-atmosphere interface through on-site measurements and a process-based MB model [Mölg and Hardy, 2004; Cullen *et al.*, 2007; Mölg *et al.*, 2008, 2009a], the possible large-scale controls by global climate model experiments [Mölg *et al.*, 2006], and mesoscale atmospheric modeling of the regional circulation over the mountain to link the two scales [Mölg *et al.*, 2009b].

In short, the climate signal of the shrinking glaciers of Kilimanjaro can be traced back to coupled atmosphere-ocean dynamics in the Indian Ocean and changes in mesoscale processes as well (e.g., stability of air masses and related dynamical and microphysical processes). Past extents of even small glaciers can therefore provide important insights into past climate dynamics, with an unexpected potential for revealing detail.

[3] There are two main difficulties in gaining a multiscale understanding. First, an approach as outlined above traverses several special disciplines of the geosciences and is challenging. Second, data sets that characterize large-scale climate dynamics over a macroregion or globally are of relatively coarse resolution (gridded observations and climate model output). Linking larger-scale climate with the cryosphere is fairly well advanced for the Greenland and Antarctic ice sheets, which are resolved in global and regional climate models due to their size [van den Broeke *et al.*, 2009; Vizcaino *et al.*, 2010]. Yet in the case of mountain glaciers, research is facing a scale problem as illustrated in Figure 1. These glaciers often reside in the scale below a few kilometers and in complex terrain, so they are difficult to resolve in large-scale data frameworks.

¹Center for Climate and Cryosphere, Institute of Meteorology and Geophysics, University of Innsbruck, Innsbruck, Austria.

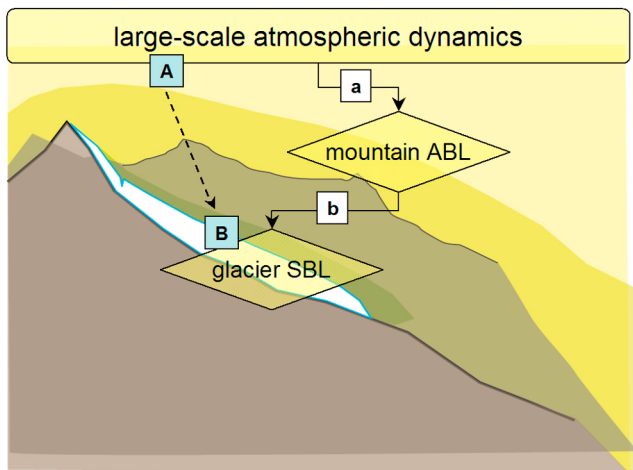


Figure 1. Sketch of how large-scale airflow, indicated by A, is modified before it is manifested locally on a mountain glacier through its mass balance, indicated by B. Mountain-airflow interactions (processes indicated by a) generate the atmospheric boundary layer (ABL) over the mountain, in which the glacier surface boundary layer (SBL) is formed through continuous exchange of energy, momentum, and mass between glacier surface and overlying air (processes indicated by b), constrained by conditions in the mountain ABL. The direct path from cause to effect (dashed line) masks multiscale linkages, which have not yet been resolved on a process level.

Recent studies referred to this as the “scale mismatch” [Machguth *et al.*, 2009; Kotlarski *et al.*, 2010].

[4] Despite this problem we have a reasonable knowledge of the relation between large-scale climate and mountain glaciers. Our most essential understanding of this was shaped by studies that made extensive regression and correlation analyses of measured MBs with indices of climate dynamics, such as El Niño and North Pacific variability [Hodge *et al.*, 1998] or the North Atlantic Oscillation [Nesje *et al.*, 2000]. These efforts also include the regression of MBs with synoptic-scale weather patterns [Yarnal, 1984; Matulla *et al.*, 2009]. Another group of studies chose to analyze the large-scale dynamical processes associated with statistical relationships [Francou *et al.*, 2003, 2004; Vuille *et al.*, 2008] and also considered the processes in the local glacier surface boundary layer (SBL) [Francou *et al.*, 2004]. The third and growing area of studies attempts to downscale large-scale circulation to the local SBL first, and then apply the local data to a glacier model. In its most basic form, these studies used grid cell values from the coarse-resolution data modified by simple statistical corrections, such as lapse rates or local scaling factors based on observations [Schneeberger *et al.*, 2001; Radić and Hock, 2006]. Others employed sophisticated statistical transfer functions for this kind of downscaling, e.g., the work of Reichert *et al.* [2001] where centuries of climate dynamics from a global climate model are linked to a mountain glacier model at the other end of the spectrum. The most recent studies considered output from regional climate models as MB forcing but also needed to link the regional and local atmospheric scale statistically by interpolation methods [Machguth *et al.*, 2009; Paul and Kotlarski, 2010]. Further, there are now

attempts to include mountain glaciers as subgrid parameterization in climate models, which allows a gross estimate of glacier volume evolution but no insights into the spatial (horizontal and vertical) variability of processes at the mountain glacier scale [Kotlarski *et al.*, 2010]. Another emerging research line is to incorporate physical principles for downscaling large-scale atmospheric patterns to local precipitation and temperature without tuning to station data [Jarosch *et al.*, 2011]. Some of these approaches have been used to calculate the response of glaciers to future climate scenarios [e.g., Radić and Hock, 2006; Matulla *et al.*, 2009].

[5] All of the examples cited above, and many others in the same area of research not mentioned here (see Machguth *et al.* [2009] for further ones), have provided important insights. None of them, however, have characterized the mesoscale processes that affect glacier behavior (Figure 1 and section 2), so a coherent process understanding of the dynamical system in Figure 1, from forcing A to response B, is not yet developed. Also, the most advanced of the previous studies were limited by the use of rather simple MB models that only required air temperature and precipitation, and occasionally solar radiation, as local forcing. In particular the lack of coherent process understanding, as well as the approach to obtain regional MB patterns [Kotlarski *et al.*, 2010], do not allow interpretation of past extents of a single glacier in terms of past climate dynamics. To our knowledge the only attempt to systematically link the different scales in a fully physical way was our approach for Kilimanjaro (see above). Yet this was not based on an integrated modeling system that could unify and deal with all these scales, but relied on different tools for different scales.

2. A Step Beyond and Goal of the Study

[6] Why is the full causality chain, A-a-b-B in Figure 1, not yet resolved on a process level in a coherent way? As indicated above, we think mainly because the mesoscale processes of airflow modifications due to mountains have barely been considered from a cryospheric viewpoint so far. Identifying these processes is a domain of dynamic meteorology, a research field on its own that does not focus on the mountain cryosphere (see Rotunno and Houze [2007] for a recent overview). Glacier-oriented studies as outlined in section 1 typically bypassed the mesoscale processes by using statistical methods.

[7] There are, however, a number of phenomena in the mesoscale that potentially affect mountain glaciers and, most probably, also affect the temporal stationarity of statistical transfer functions. Much investigated processes in dynamic meteorology are for instance general flow regimes and associated gap flows, luff and lee effects, and regional wind systems [Gohm and Mayr, 2005; Medina *et al.*, 2005; Gohm *et al.*, 2008]; the formation of gravity waves and rotors [Medina *et al.*, 2005; Doyle and Durran, 2007; Gohm *et al.*, 2008]; the impact of thermodynamic stratification of the impinging flow on smaller-scale flow features (flow blocking, splitting, and retardation) [Jiang, 2003; Mölg *et al.*, 2009b]; the nature of explicitly modeled clouds (convective versus stratiform) and related static stability [Kirshbaum and Durran, 2004; Fuhrer and Schär, 2005]; and finally, under consideration of all the aforementioned processes, the fine-scale pattern of orographic precipitation forced by the

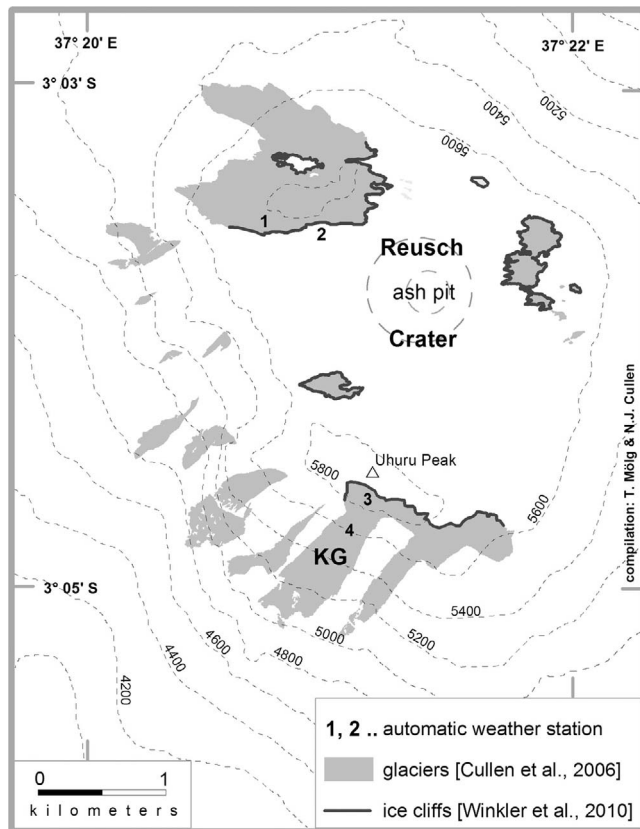


Figure 2. Map of Kilimanjaro's central part Kibo with automatic weather stations 1 (5794 m, operational since February 2000), 2 (5730 m, February 2005), 3 (5873 m, February 2005), and 4 (5600 m, October 2009). Kersten Glacier (KG) is indicated. AWS 1 is a University of Massachusetts site; the others are University of Innsbruck stations.

mountain-atmosphere interactions [Jiang, 2003; Warner *et al.*, 2003; Rotunno and Houze, 2007; Mölg *et al.*, 2009b; Wastl and Zängl, 2010]. Usually such studies employ idealized atmospheric model setups at very high spatial and temporal resolutions (e.g., bell-shaped mountains in one computational grid, horizontally homogenous forcing) or, in a realistic setup, limited area atmospheric models (LAMs) with multiple grid nesting and variable forcing at the lateral boundaries (see further below). In both cases the ultimate grid sizes in the model can be reduced to as small as a few hundred meters. To our knowledge the only study that addressed mesoscale processes from the viewpoint of glacier MB in detail was that by Mölg *et al.* [2009b], in which an idealized setup was used to examine the nature of the regional mesoscale processes, so these simulations could not be quantitatively linked to a glacier MB model.

[8] Now is the time to explore if a LAM is able to *dynamically* downscale large-scale flow to, and thus resolve, the local SBL conditions at mountain glacier scale, for their direct application to a process-resolving MB model. This yields a physically consistent framework to solve the scale problem in Figure 1 quantitatively in a coherent way, involving regional and local effects on glacier MB. Note though that grid size in a numerical atmospheric model cannot be equated with phenomenological size [e.g., Kniewel

et al., 2007], so by “resolving the mountain glacier scale” we understand the ability of the LAM to approximate the real topography closely and resolve the glacierized altitudes, and to simulate the atmospheric state at these altitudes reasonably well. We take Kilimanjaro (East Africa) as a test case and focus on two contrasting climatological periods, 1 month of the dry and 1 month of the wet season. The main goal is to explore the difference in MB model performance, and in resultant MB and energy balance patterns on a mountain glacier, between two different types of forcing data: (1) measurements from an automatic weather station (AWS) and (2) direct LAM output that is neither corrected nor adjusted statistically. A further goal is to illustrate the potential of our approach to enhance understanding of climate-glacier relations in the previously neglected meso-scale process space.

3. Methodology

3.1. Field Measurements

[9] Meteorological and glaciological measurements at high altitude on Kilimanjaro's central peak, Kibo (Figure 2), serve to (1) validate the numerical models used (see below) and (2) drive the employed MB model (section 3.4). Here we mostly consider data from AWS3 on Kersten Glacier (Figure 2), which feature incoming and outgoing components of shortwave and longwave radiation fluxes, air temperature and humidity, wind speed and direction, air pressure, and surface height change as indicator of solid precipitation and ablation. The details about these data (sensor types and accuracy, sampling frequency, quality control) are given by Mölg *et al.* [2008, 2009a, 2009b]. At lower elevation on Kersten Glacier ablation measurements from stakes exist [Mölg *et al.*, 2009a]. Details of the other AWSs on Kibo, as well as of short-term experiments during field visits (eddy covariance operations and photogrammetry), are provided by Mölg and Hardy [2004], Cullen *et al.* [2007], Kaser *et al.* [2010], and Winkler *et al.* [2010]. AWS operations in remote environment are difficult due to harsh conditions [van den Broeke *et al.*, 2004], but AWS3 data from February 2005 to January 2008 are of high quality as noted by Mölg *et al.* [2009a].

3.2. Satellite Observations

[10] We use data from the Moderate Resolution Imaging Spectroradiometer (MODIS) of the Terra and Aqua satellites, which provide a multitude of atmospheric variables at high resolution (~ 1 km), to validate simulated LAM patterns in the mesogamma scale. Specifically we look at the cloud liquid water path (LWP) data, which proved useful in the evaluation of LAMs [Fairman *et al.*, 2011]. Sampling of the Kilimanjaro region occurs between 07:10 and 08:35 UTC (Terra) and 10:15 and 11:45 UTC (Aqua). MODIS data are distributed by NASA at <http://modis.gsfc.nasa.gov/>.

3.3. Atmospheric Model

[11] We employ the Advanced Research version of the Weather Research and Forecast Model (WRF), version 3.1, to simulate circulation patterns over East Africa and Kilimanjaro. The model [Skamarock and Klemp, 2008] is three-dimensional and based on fully compressible and nonhydrostatic equations, which are solved on an Arakawa

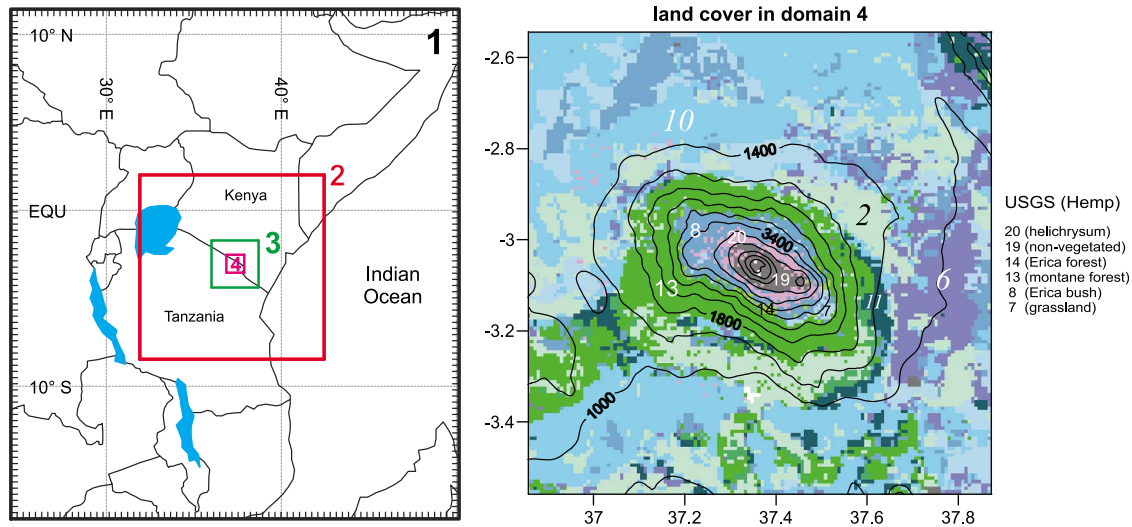


Figure 3. (left) Grid structure in the LAM. (right) The land cover types (colors) and the altitude (contours every 400 m) in domain 4. The five vegetation zones of the detailed land use accounts of *Hemp* [2005] for the year 2000 (see legend), as well as the nonvegetated summit zone, were assigned to the USGS 24-class system used by the WRF model: 13 (evergreen broadleaf forest), 14 (evergreen needleleaf forest), 8 (shrubland), 7 (grassland), 20 (herbaceous tundra), and 19 (barren). The remaining dominant categories from the standard data set are indicated in italics and different font type: 2 (dry cropland and pasture), 6 (cropland/woodland mosaic), 10 (savanna), and 11 (deciduous broadleaf forest). The three white cells in the summit zone represent the glacier areas, where bare ice (fresh snow) albedo is set to 0.3 (0.8).

C grid stagger in the horizontal and a terrain-following coordinate in the vertical. Figure 3 shows the spatial configuration of our simulations, which emerged as numerically robust from numerous preliminary runs. Multiple grid (domain) nesting allows us to decrease the grid spacing from 39 km over East Africa to 812 m over Kilimanjaro (Table 1). In grid 4 the model peak reaches an altitude of 5573 m (versus 5873 m in reality) and 18 terrain grid cells lie above the altitude where glaciers exist today (>5200 m). At the lateral boundary the model is forced by European reanalysis data [Simmons *et al.*, 2007].

[12] The WRF model features a number of options for different physical parameterizations [e.g., Luo *et al.*, 2010; Hu *et al.*, 2010]. Table 1 summarizes the options chosen here, as well as the spatial discretization sketched above. Note that we assume explicit resolution of convection in grid 4 due to the high spatial resolution [e.g., Gohm *et al.*, 2008]. Also we chose explicit numerical sixth-order diffusion to effectively damp waves at small wavelengths and prevent spurious noise [Knievel *et al.*, 2007]. Such noise becomes a problem in light wind conditions and neutral or weakly unstable boundary layers [Knievel *et al.*, 2007], which is the typical daytime case in the high elevations on Kilimanjaro [Mölg and Hardy, 2004]. Runs with implicit horizontal diffusion indeed showed a strong overestimation of AWS3 precipitation. For the lower boundary (land surface scheme) we do not use the model's standard data set but interpolate the detailed land cover data of *Hemp* [2005] to correspond to the grid of domain 4 (Figure 3).

3.4. Mass Balance Model

[13] The model is described completely by Mölg *et al.* [2009a] and belongs to the fully process-based MB mod-

els, which can be run in spatially distributed mode with a dedicated radiation scheme [e.g., Klok and Oerlemans, 2002]. Refer to Mölg and Hardy [2004] for details of the turbulence parameterization, to Mölg *et al.* [2008] for the thermodynamic subsurface scheme, and to Mölg *et al.* [2009c] for the radiation scheme. The model computes the specific MB as the sum of solid precipitation, surface melt

Table 1. User-Specific Settings in the WRF Model for the Present Study^a

Feature or Component	Setting
Horizontal grid spacing	39, 13, 3.25, 0.812 km (grids 1–4)
Layers in the vertical	terrain following (35)
Lateral boundary condition	variable (ERA-Interim ^b at 0.7°, 6-hourly)
Top boundary condition	Rayleigh damping
Grid nudging	yes (grid 1, 6-hourly), no (grids 2–4)
Long time step	180, 60, 15, and 3.75 s (grids 1–4)
Land surface	RUC scheme
Atmospheric surface layer	Monin-Obukhov scheme
Planetary boundary layer	YSU scheme (wet season), MYJ scheme (dry season)
Horizontal advection	explicit sixth-order
Cloud microphysics	Thompson scheme
Cumulus parameterization	Betts-Miller-Janjic (grids 1–3), none (grid 4)
Radiation	Dudhia (shortwave) and CAM (longwave) schemes

^aSee Skamarock and Klemp [2008] or Luo *et al.* [2010] for details and references of the schemes.

^bAlso used to define initial conditions. Simulations start 3 days before the study periods to allow for spin-up.

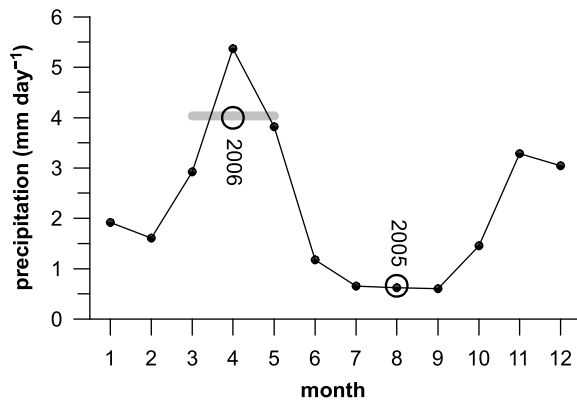


Figure 4. Mean annual cycle of precipitation in CMAP data (1979–2008) for the area covering Kilimanjaro (mean of grid cells centered at 3.75°S and 36.25°E and 38.75°E). Precipitation of the study periods is indicated by the circles, and the mean of the main wet season (March–May) is indicated by the bold gray line.

and sublimation, surface deposition, and refreezing of meltwater in the snowpack. The approach is based on the surface energy balance and the englacial temperature distribution, including energy release by penetrating solar radiation and refreezing of liquid water. The model is forced by hourly air temperature (T_a), relative humidity (RH), wind speed (V), air pressure (p), precipitation (P), and an effective cloud cover fraction (n_{eff}). In distributed MB models these values are from one reference altitude while defined vertical gradients (which are MB model parameters) and the barometric equation for p serve to extrapolate the atmospheric conditions over the entire glacier. Thus, the reference altitude is 5873 m (5573 m) for forcing with AWS3 data (LAM grid 4 output) in our case. Equation 1 and Table 1 in the work by Mölg *et al.* [2009a] provide a fast way to see the relation between forcing data, mass and energy balance components.

[14] Mölg *et al.* [2009a] ran and verified the MB model for Kersten Glacier with AWS3 data for a 3 year period (February 2005 to January 2008), using a T_a gradient of -0.0065 K m^{-1} , a V gradient of $0.0013 \text{ m s}^{-1} \text{ m}^{-1}$, and no gradients in P , RH and n_{eff} . “Verified” means the model

agreed well with measured surface height changes and MB at AWS3 as well as further downslope at ablation stakes, and with the measured glacier surface temperature at AWS3.

3.5. Study Periods

[15] We select 2 months from these 3 years, which are representative of a dry season month (August 2005) and a wet season month (April 2006) on Kilimanjaro. This choice is supported by the long record from AWS1 (D. Hardy, personal communication, 2010) as well as by the regional precipitation record from the satellite- and rain gauge-based CMAP data [Xie and Arkin, 1997] in Figure 4, where the 2 months mimic the respective mean value of the main wet season (March–May) and main dry season (July–September) accurately. Running the high-resolution LAM for a full month entails considerable computational expense, especially for data storage for the hourly output frequency. Resolving the diurnal cycle, however, is essential to modeling the MB of low-latitude glaciers [Mölg *et al.*, 2008, 2009c] and is common practice for nontropical glaciers too [Klok and Oerlemans, 2002].

[16] Figure 5 illustrates the MB characteristics of the 2 months. Sublimation dominates the mass budget of the dry season, where snowfall events are rare and melting at the surface is virtually absent. In the wet season melt dominates the ablation and removes mass from the surface together with sublimation, while frequent precipitation adds mass. This increases the mass turnover significantly in the wet season. More detailed analyses of these contrasts are given by Mölg *et al.* [2008, 2009a] or by Francou *et al.* [2004] for a different tropical site. The associated atmospheric conditions and energy fluxes will be discussed in section 4. The results in Figure 5 stem from a MB model run that was driven by AWS data. Again, the central question in this article is whether we arrive at the same causal interpretation of mass changes in the two seasons when we use scale-uncorrected LAM output to drive the MB model.

4. Results and Discussion

4.1. Simulated Atmospheric Conditions

[17] The six forcing variables for the MB model are shown in Figure 6, measured at AWS3 and simulated by the

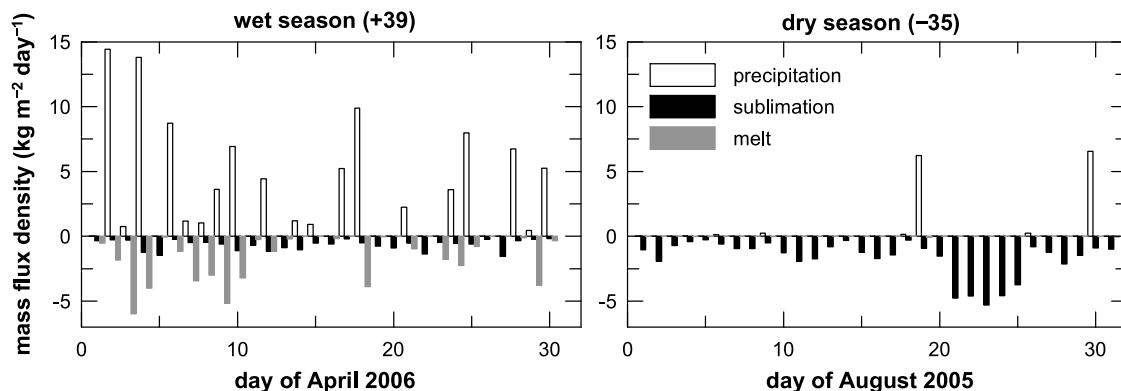


Figure 5. The main mass balance components of Kersten Glacier (area integrated) in August 2005 and April 2006: solid precipitation, surface sublimation, and surface melt. Ablation components have a negative sign, and the monthly net mass budget is shown in the titles. Data are from Mölg *et al.* [2009a].

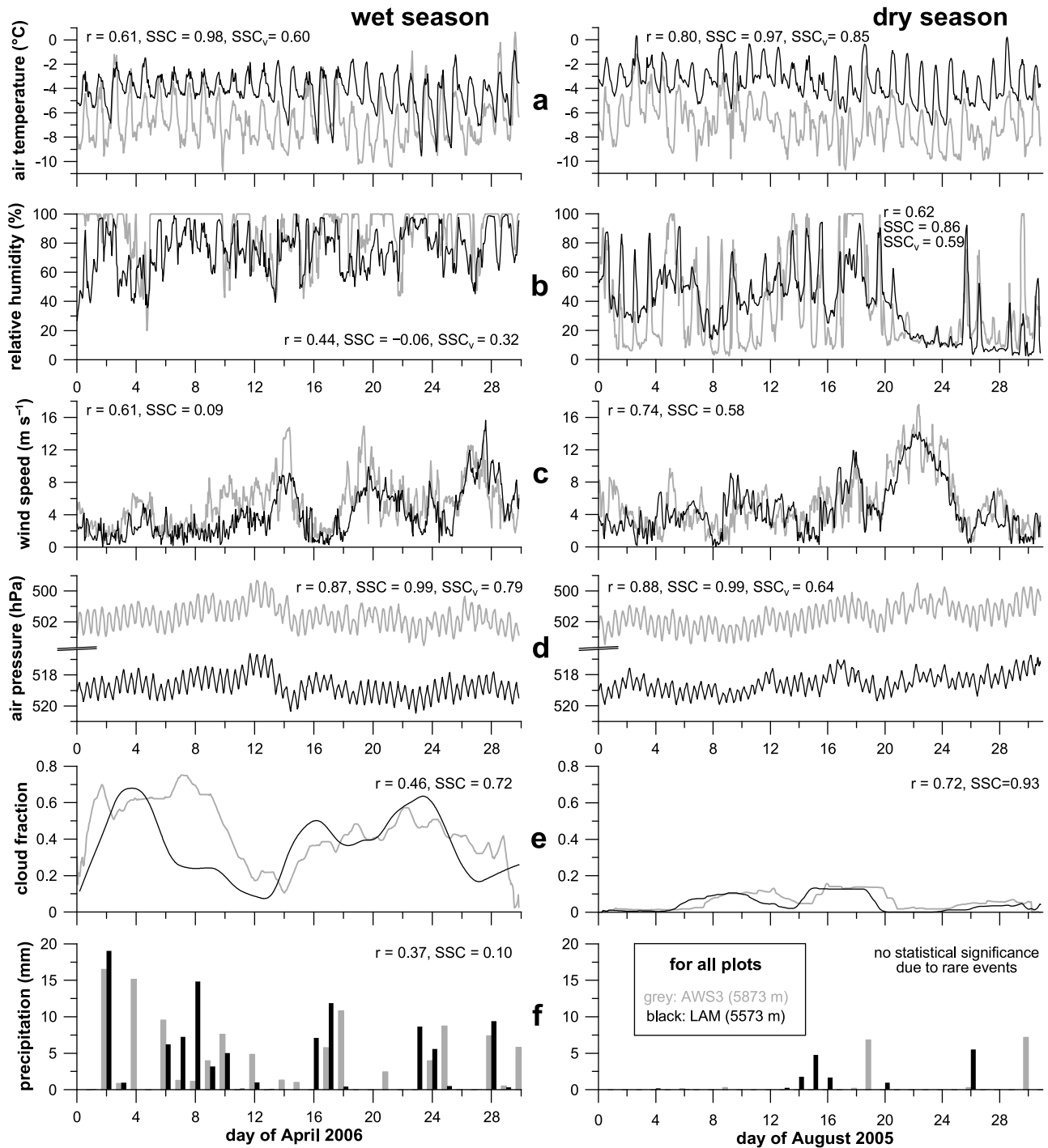


Figure 6. Hourly time series of (a) 2 m air temperature, (b) relative humidity, (c) wind speed, (d) air pressure, and (e) cloud cover fraction (5 day running mean) at AWS3 and on the LAM’s Kibo summit in domain 4 in (left) April 2006 and (right) August 2005. (f) Precipitation per day as measurements are only reliable in daily steps [Mölg and Hardy, 2004]. Displayed statistics are explained in the text. Note the altitude difference of 300 m between the two data sources.

LAM. In principle there is an appreciable or even strong correlation for all variables in both seasons, and the sharp moisture contrasts between the 2 months (RH, *P*, cloudiness) are captured well by the LAM. Strong *P* events are sometimes displaced in the model by a few days, but the simulated amounts (102 (15) mm against 109 (15) mm

measured in the wet (dry) month) as well as the magnitudes of daily *P* events are realistic.

[18] Calculating a mean bias does not make sense in our context since there is an altitude difference between actual and model summit, which can be incorporated in the subsequent MB modeling simply by a different reference alti-

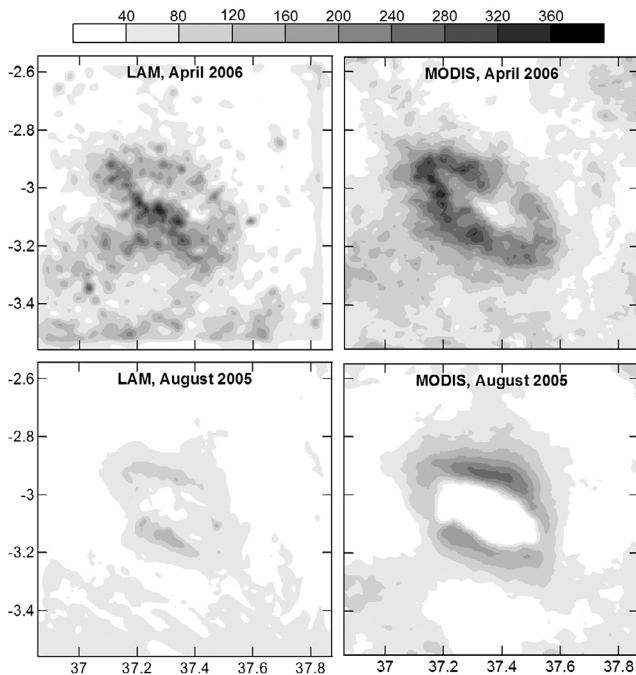


Figure 7. Cloud liquid water path (g m^{-2}) in LAM domain 4 and in MODIS data for August 2005 and April 2006. Data are averaged for all available MODIS-Terra and MODIS-Aqua overpasses and the closest hourly LAM outputs (08:00 and 11:00 UTC daily in most cases).

tude (section 3.4). We do calculate, however, a skill score (SSC) after *Wilks* [2006]: $\text{SSC} = 1 - (\text{MSE}/\text{MSE}_{\text{ref}})$, where MSE is the mean squared error between measurements and model (LAM domain 4), and MSE_{ref} between measurements and a reference model. Here the latter is the LAM output from domain 1 for Kibo summit (2060 m). The SSCs illustrate that multiple grid nesting clearly adds skill to the simulation of the observed summit conditions ($0 < \text{SSC} < 1$), except for RH in the wet season. As T_a and p decrease with altitude in the atmosphere, $\text{SSC} \approx 1$ for these variables is not unexpected, and thus we calculate another SSC (SSC_c) where the mean value is removed from all involved data sets. This test exhibits that domain 4 simulations also produce better atmospheric variability in the summit zone, and importantly this is also valid for wet season RH.

[19] Cloud cover fraction (CCF) deserves a dedicated short discussion. In the AWS forcing the “effective” CCF (n_{eff}) needs to be derived from point-measured radiation at AWS3 [Mölg *et al.*, 2009c], and similar “cloud factors” were used elsewhere for MB modeling [e.g., *Klok and Oerlemans*, 2002; *Francois et al.*, 2004]. In the LAM we extract CCF directly from the simulated hydrometeors in domain 4, by searching the air layers above the model summit (<520 hPa) in a horizontal view field of 0.5° for the maximum CCF. As in the work by *Liu and Moncrieff* [2007] we assume that a grid cell is covered by a cloud if the total condensate mixing ratio exceeds 0.01 g kg^{-1} . Most important for the MB modeling is a good representation of clouds during hours with solar insolation [Mölg *et al.*, 2009c], for which good agreement exists between the mean values of n_{eff} (0.32/0.07 in wet/dry season) and LAM CCF (0.36/0.05). The 0.5° in the algorithm are arbitrary but widening

the search area only incorporates distant clouds, which affect insolation at low sun elevation and, thus, have a small effect on the daily solar radiation budget on the summit. The hourly n_{eff} and LAM CCF curves show hardly any correlation since both strongly fluctuate, but smoothing over a few days as in Figure 6e reveals basic agreement and unfolds an interesting fact: the radiation-derived “cloud factors” commonly used in MB modeling appear to reasonably represent the atmospheric cloud field simulated from physical principles. CCF in domain 1 (for the SSC calculation) was determined as subgrid phenomenon with the RH-based parameterization by *Xu and Randall* [1996] again for air layers <520 hPa, but is much less suited as MB model forcing than explicitly simulated cloudiness in domain 4 (see high SSCs in Figure 6e).

[20] The reference MB calculations [Mölg *et al.*, 2009a] assume the absence of a vertical P gradient on Kersten Glacier (though a possible P gradient was included in the uncertainty estimate of the 2009 paper). However, should P decrease with elevation in the summit zone as it does at lower elevations [Hemp, 2006], which will be revealed once a longer combined AWS3/AWS4 record is available, P on the model summit (5573 m) should be higher than at AWS3 (5873 m). This could easily be achieved by reasonable measures, for instance by the choice of the PBL scheme [Hu *et al.*, 2010], the microphysics scheme [Luo *et al.*, 2010], or by lowering the sixth-order diffusion strength (a consistent result in our preliminary runs). In this sense we also varied the PBL scheme between the seasons (Table 1), because the wet season setup produced too little P on the summit in the dry season. This illustrates the advantage of a LAM, which is to provide different physics schemes for particular climatic circumstances.

[21] While the centerpiece of our interest concerns the simulated atmospheric conditions on Kibo summit, Figure 7 extends to the spatial performance of the LAM. The sharp seasonal difference in LWP is simulated by the LAM, and the main characteristics of the spatial LWP patterns as well. The characteristic dry season concentrations of LWP on the northern and southern mountain slopes, which were referred to as “cloud banks” [Fairman *et al.*, 2011], are less pronounced though in the LAM. This applies mostly to the northerly slopes, which also emerged in a dry season 2007 simulation with a different LAM [Fairman *et al.*, 2011]. Thus there is either a more general LAM problem for this specific detail or the MODIS data overestimate the LWP. In summary, however, the gross features of the spatial moisture patterns are consistent between the two data sources, and for the summit zone the LAM adds skill through multiple grid nesting and characterizes the seasonal climate features reasonably. The central question now is whether this performance is good enough for direct usage of LAM output in high-resolution MB modeling.

4.2. Uncorrected LAM Output as MB Model Input

[22] Figure 8 clearly affirms this question, where the total MBs modeled by LAM forcing show the same overall result as the MBs obtained from AWS3 forcing. Owing to differences in the variability of the two forcing data sets (Figure 6) there are expected discrepancies on certain days, in particular due to the different timing of precipitation events. In the dry season, for instance, the LAM produces

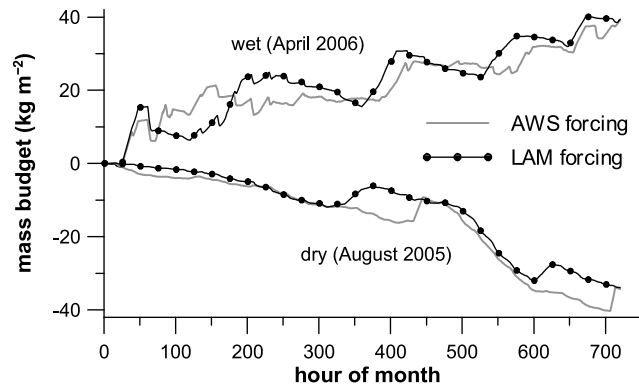


Figure 8. Modeled accumulated total MB on Kersten Glacier in August 2005 and April 2006 from two different forcing types: AWS3 data (5873 m) and LAM domain 4 output for Kibo summit (5573 m). The AWS driven run was verified with independent measurements by Mölg *et al.* [2009a].

the two wet spells in the middle and toward the end of the simulation period with the right magnitude but a few days too early, which is reflected in the accumulated MB curve. Ablation, on the other hand, coincides in several instances even for detailed aspects, like in the dry season from hour 500–600 when the sublimation-driven ablation is intensified (due to high wind speeds, see Figure 6c). On the monthly scale, both the MB magnitude and its general evolution in time are robust in the two seasons regardless of the forcing type.

[23] Good accordance does not necessarily mean that the causal interpretation of the total mass changes in Figure 8 is the same from the two forcing types, as there could be compensating differences in the MB components. Figure 9 therefore resolves the MB and surface energy balance terms. LAM forcing shows less pronounced difference between melt and sublimation in the wet season than AWS forcing, since the lower RH in the LAM (Figure 6b) leads to a stronger turbulent latent heat flux away from the surface (Figure 9, right). Sublimation therefore expends a greater fraction of the available energy, but we still obtain more

melt than sublimation in the wet season through LAM forcing. In all other aspects there is strong agreement, so again we can draw a robust conclusion, this time about the causal factors that shape the total MB.

[24] These results are promising, since they show a path to downscale large-scale dynamics to realistic magnitudes of energy and mass fluxes on a small high-altitude glacier in a fully process-based way. The key in our case was to achieve a resolution of ~ 1 km in the LAM for a realistic precipitation simulation in the summit zone. From output of LAM domain 3 (~ 3 km resolution) the agreement in Figure 8 could not be reached, as P is grossly overestimated: the model summit lies in a too low and therefore too moist elevation zone, and the cumulus parameterization introduces additional uncertainty. Refinement of the land cover (Figure 3) had a positive but less crucial effect on the summit's SBL simulation, and so did the precise choice (± 0.1) of albedo thresholds for the glacier cells. In future, MB models could even become a part of LAMs and be fully interactive, which can be neglected for small mountain glaciers like Kersten but could ensure realistic feedbacks of the glacier SBL on the mountain's ABL in the case of large ice caps.

4.3. Mesoscale Processes

[25] Besides providing realistic forcing data for MB modeling, the greatest advantage of high-resolution LAM simulations from a glaciological viewpoint is to help us (1) understand the physics of mesoscale processes that affect glacier mass and (2) identify from them possible relations to the larger-scale flow, which could aid the development of multiscale parameterizations of the atmosphere-cryosphere system (section 4.4). While this paper focuses on the LAM effectiveness for MB modeling, we want to at least illustrate the potential for items 1 and 2 using the well-known concept of diurnal circulation and resultant cloudiness on tropical mountains: downslope flow with low-altitude clouds during the night, and insolation-driven upslope flow with cloud growth along mountain slopes during daytime. Troll and Wien [1949] scrutinized this idea decades ago, and it was reconsidered repeatedly in subsequent studies [e.g., Davies *et al.*, 1979; Mölg *et al.*, 2003].

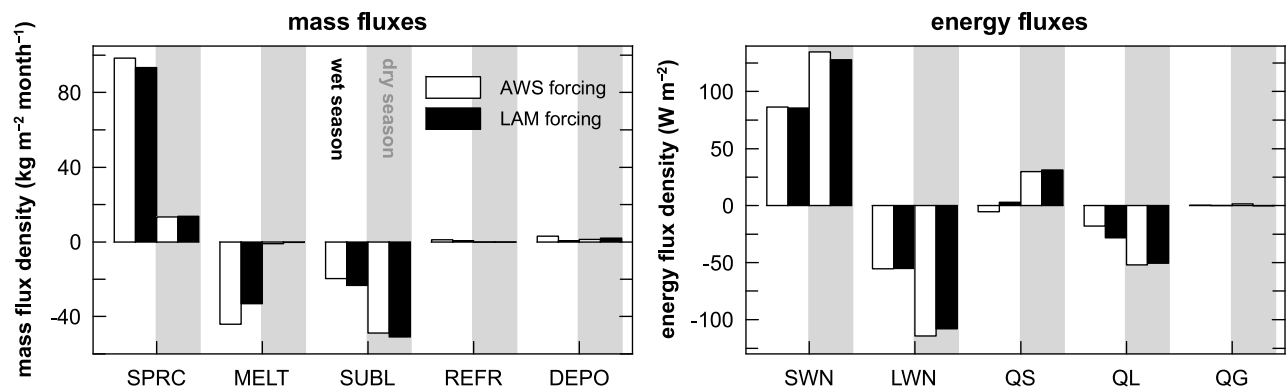


Figure 9. Modeled total MB and energy balance components on Kersten Glacier in August 2005 (gray background) and April 2006 (white background) from two different forcing types: AWS3 data (5873 m) and LAM domain 4 output for Kibo summit (5573 m). Solid precipitation (SPRC), surface melt and sublimation (MELT and SUBL), internal refreezing (REFR), surface deposition (DEPO), net shortwave and net longwave radiation (SWN and LWN), turbulent sensible and latent heat flux (QS and QL), and ground heat flux (QG).

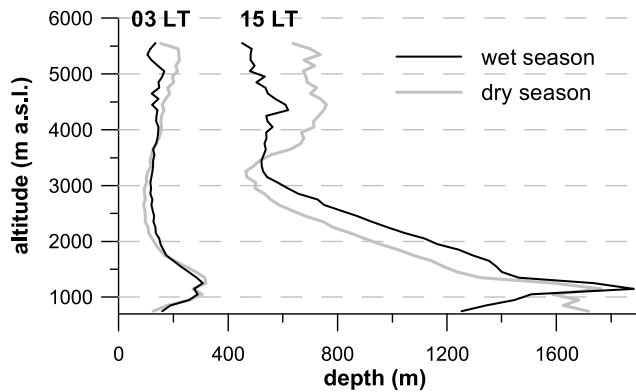


Figure 10. Mean ABL depth versus terrain altitude in domain 4 in August 2005 and April 2006 at 03:00 and 15:00 LT. The lateral buffer zone of the domain (five grid points) is excluded from the analysis.

[26] We begin by analyzing the ABL depth over the mountain to get a sense for the impact of the terrain on the atmospheric flow (Figure 10). Strong growth of the mixed layer height (i.e., the daytime ABL depth) is evident at low elevations, but even over the summit zone the depth reaches 500–750 m. From a seasonal perspective mean solar insolation at the surface is larger at all elevations in the dry season, with greatest differences above 3000 m where the ABL is thicker than in the wet season. At lower elevations, however, higher moisture content in the wet season overcompensates the radiation effect and makes the ABL mostly deeper. Henceforth we will focus on the wet season simulation, which is more interesting physically due to the greater importance of moist dynamics.

[27] Figure 11 compares the diurnal evolution of clouds in the April 2006 simulation. On days with no summit precipitation (NOSUP) as well as on days with summit precipitation (SUP; >1 mm) the concept of *Troll and Wien* [1949] emerges: clouds over the terrain are confined to the layers below ~700 hPa at night and ascend during the day.

The strongest rise occurs between 10:00 and 12:00 LT and leaves the low altitudes cloud free until after sunset. Cirrus clouds are present in the free atmosphere, but the pivotal difference between SUP and NOSUP composites is the weak cloudiness of the 550–400 hPa layer in the NOSUP case. In contrast, deep clouds evolve on SUP days. This has implications for the glacierized altitudes (550–500 hPa), where the difference in clouds maximizes shortly after midday but reappears late in the day after 19:00 LT (Figure 11, right).

[28] To elaborate this difference, Figure 12 extends to the hydrometeor composition of the clouds. Cirrus are dominated by snow in both cases, while rain is the only precipitable hydrometeor species from ~600 hPa downward. Precipitation in the glacier zone during SUP is also dominated by snow but includes fractions of graupel and rain, which are the three species we witnessed in Kilimanjaro's summit zone during field trips [e.g., *Mölg et al.*, 2009b]. Snow is also the key to understanding the lack of high-elevation precipitation on NOSUP days: while the cirrus shields in both cases contain abundant snow, a sharp transition to snow-free layers below 500 hPa appears in the NOSUP case. This suggests that falling snow sublimates in NOSUP cases before it reaches the glacierized elevations or, more likely, that there is insufficient convection from beneath to form precipitation on the summit.

[29] Clearest differences in cloud-related processes are detectable shortly before noon, which is followed by the mentioned maximum difference in cloudiness (Figure 11, right). This is exemplified in Figure 13 through the moist Brunt-Väisälä frequency (N_m^2), which is an indicator of static stability in saturated air and the appropriate metric to diagnose convective cellularity [*Kirshbaum and Durran*, 2004], the horizontal moisture flux convergence (MFC; positive defined as convergence) and the moist static energy (s_e). These quantities are calculated as done by *Mölg et al.* [2009b], from *Banacos and Schultz* [2005] and *Pielke* [2004]. At 10:00 LT a salient feature is drastically reduced instability of the clouds at 640–630 hPa during NOSUP (Figure 13a). This thin layer even contains statically stable

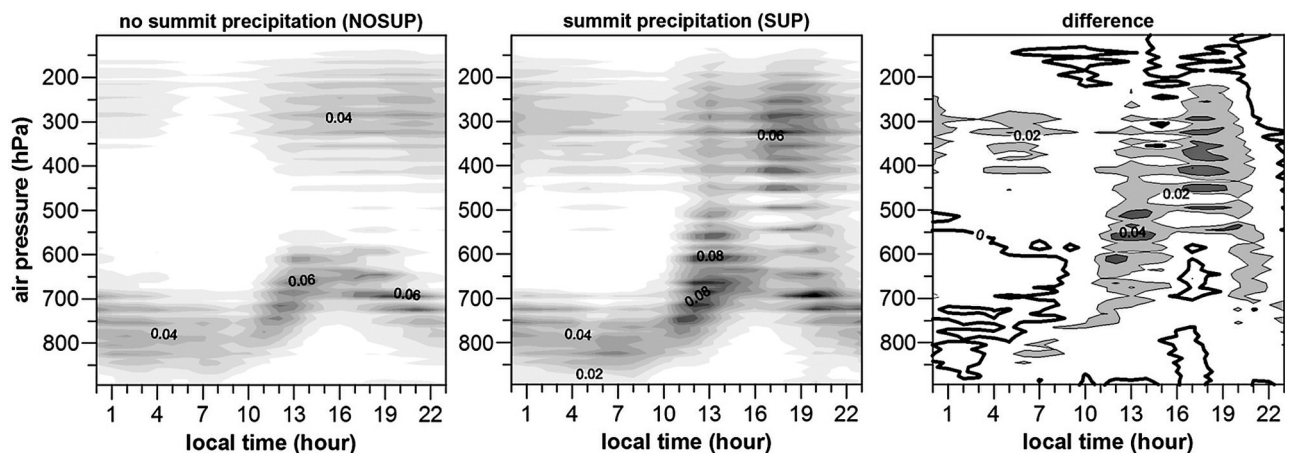


Figure 11. Domain averaged profiles (bin size 10 hPa) of the diurnal cycle of total condensate mixing ratio in domain 4 for NOSUP and SUP days in the wet season simulation (filled contours every 0.01 g kg^{-1}). The difference plot employs 0.02 g kg^{-1} spacing (zero contour is bold). The lateral buffer zone of the domain (five grid points) is excluded from the analysis.

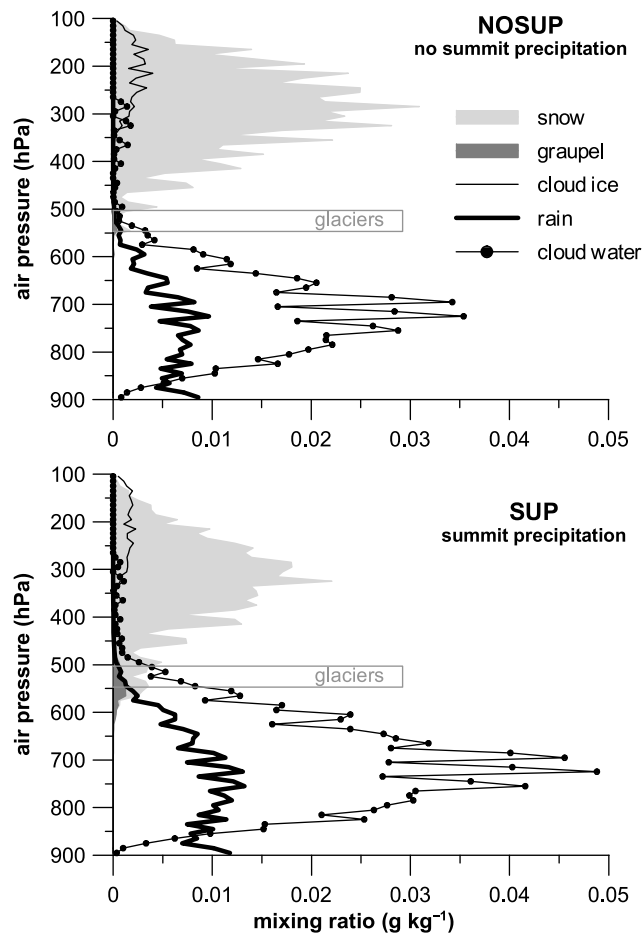


Figure 12. Time and domain averaged profiles (bin size 10 hPa) of cloud water, cloud ice, rain, snow, and graupel mixing ratios in domain 4 for NOSUP and SUP days in the wet season simulation. The lateral buffer zone of the domain (five grid points) is excluded from the analysis. The elevation range of the presently glacierized summit zone is indicated by the rectangle.

flow ($N_m^2 > 0$), which is masked by the layer mean value in Figure 13a. SUP shows greater instability throughout 650–500 hPa, i.e., exactly in Kilimanjaro’s highest-elevation zones. The almost stable layer at ~ 635 hPa during NOSUP also marks the transition to clearly reduced MFC in the summit zone at 11:00 LT (Figure 13b), and the major difference in the SBL moist entropy field at 12:00 LT exists above 4500 m and grows toward the mountain summit (Figure 13c).

[30] The processes discussed not only provide insight into mesoscale dynamics that affect high-altitude precipitation and thus the MB of mountain glaciers, but also illuminate local vertical gradients in meteorological elements above the glacier surface. Cloud processes, for instance, influence vertical gradients in moisture and precipitation (see above), but also in wind speed due to convective activity [Mölg *et al.*, 2009b] and in air temperature as a result of diabatic processes during water phase changes [Liu and Moncrieff, 2007]. All these gradients are required for distributed MB modeling. They are usually incorporated as time-invariant parameters [Klok and Oerlemans, 2002; Reijmer and Hock, 2008; Mölg *et al.*, 2009a], which could be reconsidered in future as suggested by the seasonal gradients in Table 2 (e.g., for MB uncertainty estimates). RH and V gradients are very small in the simulations, but for T_a and P they do show seasonal variability (Table 2). In addition to the vertical gradients (Figures 11–13), horizontal gradients exist as well that can equally be diagnosed from LAM output. In any case the examples in this section demonstrate that similar process understanding can certainly not be gained from coarse-resolution data that were generated without explicit resolution of clouds or with insufficient terrain detail.

4.4. Transferability of the Concept and Research Benefit

[31] Kilimanjaro is certainly not a typical glacierized mountain due to its location at the equator, its small glaciers that are confined to the summit zone, and its free-standing character. The latter two in combination constrain the spatial variability in ABL depth over the glacierized zone (Figure 10), and might ameliorate the simulation of a local SBL from

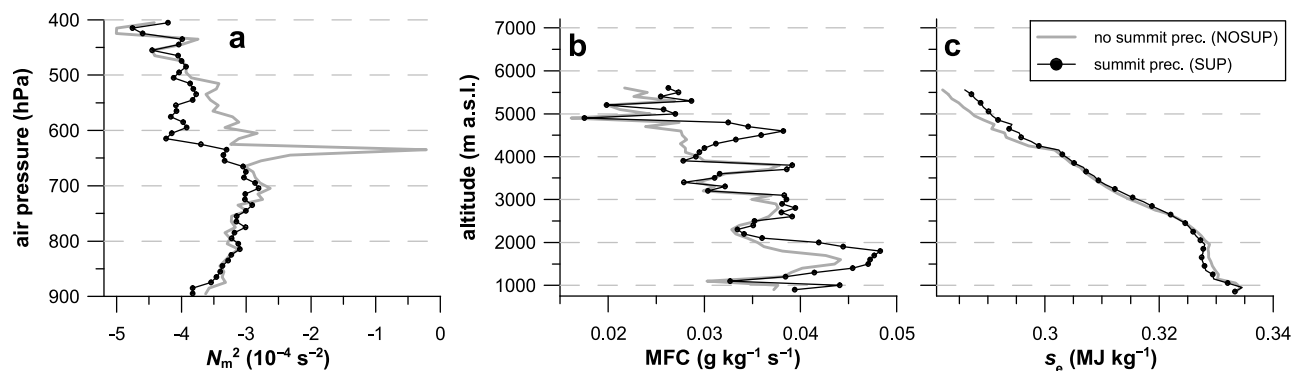


Figure 13. Domain averaged profiles of (a) squared moist buoyancy frequency (N_m^2) at 10:00 LT in the cloud regions (bin size is 10 hPa), (b) near-surface maximum horizontal moisture flux convergence (MFC, model level 1) at 11:00 LT, and (c) 2 m moist static energy (s_e) at 12:00 LT in domain 4 for NOSUP and SUP days in the wet season simulation. The lateral buffer zone of the domain (five grid points) is excluded from the analysis. The range of the altitude axes (bin size 100 m) corresponds to the air pressure range in Figure 13a.

Table 2. Simulated Mean Vertical Gradients in Meteorological Conditions Between the Two Glacier Grid Cells That Represent the Southern Ice Field in Domain 4 (5213 and 5573 m)

Gradient per 100 m	August 2005 (Dry Season)	April 2006 (Wet Season)
Air temperature (°C)	-0.56	-0.71
Relative humidity (% units)	-1.3	+0.5
Wind speed (m s ⁻¹)	+0.2	+0.2
Precipitation (mm month ⁻¹)	+0.2	-3.2

large-scale forcing. We surmise that glacier SBL modeling becomes more complicated for larger alpine glaciers that flow into valleys. The ABL structure in mountain valleys is probably more complex than on Kilimanjaro, since its depth can vary significantly due to small-scale secondary flow patterns that are hard to simulate [Weigel *et al.*, 2006]. In addition, large valley glaciers exert a notable impact on the local SBL especially during dry weather [Konya and Matsumoto, 2010], compared to small glaciers that are exposed to the free tropospheric flow. On the other hand, an isolated high mountain like Kilimanjaro entails a larger elevation difference between adjacent grid cells than a gradually up-building terrain of much wider horizontal dimension, thus representing adverse conditions for numerical stability in a LAM [Pielke, 2002]. Also, patterns of precipitation are more localized and harder to simulate in convective cases (like on Kilimanjaro) than in stable cases [Rotunno and Houze, 2007] which might dominate elsewhere. Thus our test case incorporates both advantages and disadvantages to the modeling approach, so we assume the concept presented can also work for glaciers of interest in other mountain ranges of the Earth.

[32] Regardless of the exact physiogeographic setting, atmospheric modeling over mountains is computationally expensive due to the high resolution required. Subkilometer resolution in the LAM target area seems vital to the concept of this study (section 4.2), and is crucial in general for successful ABL modeling over complex terrain [Rotach and Zardi, 2007]. Here we considered 2 months for contrasting seasons, which demanded numerous runs to determine an appropriate setup of the LAM. Once this is found, however, simulating several seasons (e.g., for average and extreme conditions in different years) is feasible and would be a great complement to long-term quantifications of the atmosphere–mountain cryosphere system, which still need to rely on statistical components (section 1). In particular, multiscale process understanding could resolve why statistical relations between large-scale climate dynamics and glacier MB are unstable over time [Hodge *et al.*, 1998; Vuille *et al.*, 2008], which pertains to the assessment of mountain glacier response to future climate. Also in this respect, insights into large-scale to mesoscale atmospheric dynamics that affect glacier MB processes and related gradients in local meteorological elements (section 4.3) could help introduce new predictors to statistical transfer functions, which would enhance their physical foundation.

[33] For backward problems, enhanced multiscale process understanding could improve the extraction of climate signals from past glacier extents significantly, including mesoscale dynamics. This would fill the gap between backward modeling that focused on the local climate [e.g.,

Yamaguchi *et al.*, 2008] or inferred large-scale dynamical changes by “trial and error” techniques [Kull and Grosjean, 2000; Mölg *et al.*, 2009a]. The prospect of extracting a climate signal with higher detail and confidence than at present clarifies one thing: small mountain glaciers can also be valuable research objects for climate science.

5. Conclusions and Outlook

[34] We have shown that the WRF LAM is an appropriate tool to dynamically downscale large-scale circulation to high-altitude meteorological conditions over a glacier, which enables their direct use (without statistical correction) in forcing a process-based MB model. This means the same causal interpretation of glacier mass variability (i.e., the same patterns of energy and MB terms) is obtained as in the case of forcing by on-site measurements. The simulated MB forcing comprises T_a , RH, \mathbf{V} and p in the SBL over the glacier, precipitation at its surface, and explicitly modeled clouds in the glacier’s view field. Suitability of the latter, in our case, supports the commonly used “cloud factor” parameter in MB modeling.

[35] Our results demonstrate that it is possible to quantify glacier mass response to large-scale atmospheric dynamics without statistical downscaling or subgrid glacier parameterizations, a novelty compared to former multiscale approaches (section 2). This success mainly relies on the high resolution of the LAM over the target area and the associated precipitation simulation, which also profited from the possibility to switch physical schemes for different seasons. Yet there are disadvantages to the approach presented here. First, atmospheric modeling over steep and high terrain is numerically tricky [e.g., Zängl *et al.*, 2004] and, at the subkilometer scale, not established in climate-cryosphere research. Second, such high-resolution modeling is computationally expensive and not yet suited for decade- or century-long simulations that are achieved with inclusion of statistical downscaling [e.g., Reichert *et al.*, 2001].

[36] Still, we suggest that our physical approach should be pursued increasingly in future research on the link between ocean, atmosphere, and alpine cryosphere in the form of time slice experiments. This offers notable advantages for the process understanding of forward and backward problems related to the mass balance of mountain glaciers, e.g., mass loss and associated potentials for sea level contribution and regional hazards [Kaser *et al.*, 2006; Fischer *et al.*, 2006]; climate reconstructions from past glaciations [Yamaguchi *et al.*, 2008]; ice core research [Hardy *et al.*, 2003]; attribution studies [Mölg *et al.*, 2006]; and in general how “the glacier SBL filters the large-scale climate signals” [Oerlemans, 2000]; Last the approach would also help to better emphasize the dynamics of *weather* in the climate research arena, which tends to neglect such short-term fluctuations.

[37] **Acknowledgments.** This research was supported by the Austrian Science Foundation (FWF, grants P2008-N90 and P21288-N10) and the University of Innsbruck’s “Nachwuchsförderung.” The supercomputing was supported by the Austrian Ministry of Science BMWF as part of the “UniInfrastrukturprogramm” of the “Forschungsplattform” Scientific Computing at LFU Innsbruck. We thank Martin Großhauser, who prepared MODIS data; Andreas Hemp, who provided vegetation data and helped to translate them to USGS classes; Alexander Gohm and Georg Mayr for their

vital advices on mesoscale modeling over recent years; Tanzanian authorities for research permission (COSTECH, KINAPA, TANAPA, TAWIRI); and Nicolas J. Cullen, Douglas R. Hardy, and Michael Winkler for leading the field work on Kilimanjaro.

References

- Banacos, P. C., and D. M. Schultz (2005), The use of moisture flux convergence in forecasting convective initiation: Historical and operational perspectives, *Weather Forecast.*, *20*, 351–366, doi:10.1175/WAF858.1.
- Cullen, N. J., T. Mölg, G. Kaser, K. Hussein, K. Steffen, and D. R. Hardy (2006), Kilimanjaro Glaciers: Recent areal glacier extent from satellite data and new interpretation of observed 20th century retreat rates, *Geophys. Res. Lett.*, *33*, L16502, doi:10.1029/2006GL027084.
- Cullen, N. J., T. Mölg, G. Kaser, K. Steffen, and D. R. Hardy (2007), Energy-balance model validation on the top of Kilimanjaro, Tanzania, using eddy covariance data, *Ann. Glaciol.*, *46*, 227–233, doi:10.3189/172756407782871224.
- Davies, T. D., C. E. Vincent, and P. Brimblecombe (1979), Condensation nuclei and weather on Mount Kenya, *J. Appl. Meteorol.*, *18*, 1239–1243, doi:10.1175/1520-0450(1979)018<1239:CNAWOM>2.0.CO;2.
- Doyle, J. D., and D. R. Durran (2007), Rotor and sub-rotor dynamics in the lee of three-dimensional terrain, *J. Atmos. Sci.*, *64*, 4202–4221, doi:10.1175/2007JAS2352.1.
- Fairman, J. G., U. S. Nair, S. A. Christopher, and T. Mölg (2011), Land use change impacts on regional climate over Kilimanjaro, *J. Geophys. Res.*, *116*, D03110, doi:10.1029/2010JD014712.
- Fischer, L., A. Käb, C. Hugel, and J. Noetzli (2006), Geology, glacier retreat and permafrost degradation as controlling factors of slope instabilities in a high-mountain rock wall: The Monte Rosa east face, *Nat. Hazards Earth Syst. Sci.*, *6*, 761–772, doi:10.5194/nhess-6-761-2006.
- Francou, B., M. Vuille, P. Wagnon, J. Mendoza, and J. E. Sicart (2003), Tropical climate change recorded by a glacier in the central Andes during the last decades of the 20th century: Chacaltaya, Bolivia, 16°S, *J. Geophys. Res.*, *108*(D5), 4154, doi:10.1029/2002JD002959.
- Francou, B., M. Vuille, V. Favier, and B. Cáceres (2004), New evidence for an ENSO impact on low-latitude glaciers: Antizana 15, Andes of Ecuador, 0°28'S, *J. Geophys. Res.*, *109*, D18106, doi:10.1029/2003JD004484.
- Fuhrer, O., and C. Schär (2005), Embedded cellular convection in moist flow past topography, *J. Atmos. Sci.*, *62*, 2810–2828, doi:10.1175/JAS3512.1.
- Gohm, A., and G. J. Mayr (2005), Numerical and observational case-study of a deep Adriatic bora, *Q. J. R. Meteorol. Soc.*, *131*, 1363–1392, doi:10.1256/qj.04.82.
- Gohm, A., G. J. Mayr, A. Fix, and A. Giez (2008), On the onset of bora and the formation of rotors and jumps near a mountain gap, *Q. J. R. Meteorol. Soc.*, *134*, 21–46, doi:10.1002/qj.206.
- Hardy, D. R., M. Vuille, and R. S. Bradley (2003), Variability of snow accumulation and isotopic composition on Nevado Sajama, Bolivia, *J. Geophys. Res.*, *108*(D22), 4693, doi:10.1029/2003JD003623.
- Hemp, A. (2005), Climate change driven forest fires marginalize the impact of ice cap wasting on Kilimanjaro, *Global Change Biol.*, *11*, 1013–1023, doi:10.1111/j.1365-2486.2005.00968.x.
- Hemp, A. (2006), Vegetation of Kilimanjaro: Hidden endemics and missing bamboo, *Afr. J. Ecol.*, *44*, 305–328, doi:10.1111/j.1365-2028.2006.00679.x.
- Hodge, S. M., D. C. Trabant, R. M. Krimmer, T. A. Heinrichs, R. S. March, and E. G. Josberger (1998), Climate variations and changes in mass of three glaciers in western North America, *J. Clim.*, *11*, 2161–2179, doi:10.1175/1520-0442(1998)011<2161:CVACIM>2.0.CO;2.
- Hu, X. M., J. W. Nielsen-Gammon, and F. Zhang (2010), Evaluation of three planetary boundary layer schemes in the WRF model, *J. Appl. Meteorol. Climatol.*, *49*, 1831–1844, doi:10.1175/2010JAMC2432.1.
- Jarosch, A. H., F. S. Anslow, and G. K. C. Clarke (2011), High-resolution precipitation and temperature downscaling for glacier models, *Clim. Dyn.*, doi:10.1007/s00382-010-0949-1, in press.
- Jiang, Q. (2003), Moist dynamics and orographic precipitation, *Tellus, Ser. A*, *55*, 301–316.
- Kaser, G., J. G. Cogley, M. B. Dyurgerov, M. F. Meier, and A. Ohmura (2006), Mass balance of glaciers and ice caps: Consensus estimates for 1961–2004, *Geophys. Res. Lett.*, *33*, L19501, doi:10.1029/2006GL027511.
- Kaser, G., T. Mölg, N. J. Cullen, D. R. Hardy, and M. Winkler (2010), Is the decline of ice on Kilimanjaro unprecedented in the Holocene?, *Holocene*, *20*, 1079–1091, doi:10.1177/0959683610369498.
- Kirshbaum, D. J., and D. R. Durran (2004), Factors governing cellular convection in orographic precipitation, *J. Atmos. Sci.*, *61*, 682–698, doi:10.1175/1520-0469(2004)061<0682:FGCCIO>2.0.CO;2.
- Klok, E. J., and J. Oerlemans (2002), Model study of the spatial distribution of the energy and mass balance of Morteratschgletscher, Switzerland, *J. Glaciol.*, *48*, 505–518, doi:10.3189/172756502781831133.
- Kniviel, J. C., G. H. Bryan, and J. P. Hacker (2007), Explicit numerical diffusion in the WRF model, *Mon. Weather Rev.*, *135*, 3808–3824, doi:10.1175/2007MWR2100.1.
- Konya, K., and T. Matsumoto (2010), Influence of weather conditions and spatial variability on glacier surface melt in Chilean Patagonia, *Theor. Appl. Climatol.*, *102*, 139–149, doi:10.1007/s00704-009-0248-0.
- Kotlarski, S., D. Jacob, R. Podzum, and F. Paul (2010), Representing glaciers in a regional climate model, *Clim. Dyn.*, *34*, 27–46, doi:10.1007/s00382-009-0685-6.
- Kull, C., and M. Grosjean (2000), Late Pleistocene climate conditions in the North Chilean Andes drawn from a glacier-climate model, *J. Glaciol.*, *46*, 622–632, doi:10.3189/172756500781832611.
- Liu, C., and M. W. Moncrieff (2007), Sensitivity of cloud-resolving simulations of warm-season convection to cloud microphysics parameterizations, *Mon. Weather Rev.*, *135*, 2854–2868, doi:10.1175/MWR3437.1.
- Luo, L., Y. Wang, H. Wang, Y. Zheng, and H. Morrison (2010), Modeling convective-stratiform precipitation processes on a Mei-Yu front with the Weather Research and Forecasting model: Comparison with observations and sensitivity to cloud microphysics, *J. Geophys. Res.*, *115*, D18117, doi:10.1029/2010JD013873.
- Machguth, H., F. Paul, S. Kotlarski, and M. Hoelzle (2009), Calculating distributed glacier mass balance for the Swiss Alps from regional climate model output: A methodical description and interpretation of the results, *J. Geophys. Res.*, *114*, D19106, doi:10.1029/2009JD011775.
- Matulla, C., E. Watson, S. Wagner, and W. Schöner (2009), Downscaled GCM projections of winter and summer mass balance for Peyto Glacier, Alberta, Canada (2000–2100) from ensemble simulations with ECHAM5-MPIOM, *Int. J. Climatol.*, *29*, 1550–1559, doi:10.1002/joc.1796.
- Medina, S., B. F. Smull, R. A. Houze Jr., and M. Steiner (2005), Cross-barrier flow during orographic precipitation events: Results from MAP and IMPROVE, *J. Atmos. Sci.*, *62*, 3580–3598, doi:10.1175/JAS3554.1.
- Mölg, T., and D. R. Hardy (2004), Ablation and associated energy balance of a horizontal glacier surface on Kilimanjaro, *J. Geophys. Res.*, *109*, D16104, doi:10.1029/2003JD004338.
- Mölg, T., C. Georges, and G. Kaser (2003), The contribution of increased incoming shortwave radiation to the retreat of the Rwenzori Glaciers, East Africa, during the 20th century, *Int. J. Climatol.*, *23*, 291–303, doi:10.1002/joc.877.
- Mölg, T., M. Renold, M. Vuille, N. J. Cullen, T. F. Stocker, and G. Kaser (2006), Indian Ocean Zonal Mode activity in a multicentury integration of a coupled AOGCM consistent with climate proxy data, *Geophys. Res. Lett.*, *33*, L18710, doi:10.1029/2006GL026384.
- Mölg, T., N. J. Cullen, D. R. Hardy, G. Kaser, and L. Klok (2008), Mass balance of a slope glacier on Kilimanjaro and its sensitivity to climate, *Int. J. Climatol.*, *28*, 881–892, doi:10.1002/joc.1589.
- Mölg, T., N. J. Cullen, D. R. Hardy, M. Winkler, and G. Kaser (2009a), Quantifying climate change in the tropical mid-troposphere over East Africa from glacier shrinkage on Kilimanjaro, *J. Clim.*, *22*, 4162–4181, doi:10.1175/2009JCLI2954.1.
- Mölg, T., J. H. C. Chiang, A. Gohm, and N. J. Cullen (2009b), Temporal precipitation variability versus altitude on a tropical high mountain: Observations and mesoscale atmospheric modeling, *Q. J. R. Meteorol. Soc.*, *135*, 1439–1455, doi:10.1002/qj.461.
- Mölg, T., N. J. Cullen, and G. Kaser (2009c), Solar radiation, cloudiness and longwave radiation over low-latitude glaciers: Implications for mass balance modeling, *J. Glaciol.*, *55*, 292–302, doi:10.3189/002214309788608822.
- Nesje, A., L. Oyvind, and S. O. Dahl (2000), Is the North Atlantic Oscillation reflected in Scandinavian glacier mass balance records?, *J. Quat. Sci.*, *15*, 587–601, doi:10.1002/1099-1417(200009)15:6<587::AID-JQS533>3.0.CO;2-2.
- Oerlemans, H. (2000), Analysis of a 3 year meteorological record from the ablation zone of Morteratschgletscher, Switzerland: Energy and mass balance, *J. Glaciol.*, *46*, 571–579, doi:10.3189/172756500781832657.
- Paul, F., and S. Kotlarski (2010), Forcing a distributed glacier mass balance model with the regional climate model REMO. Part II: Downscaling strategy and results for two Swiss glaciers, *J. Clim.*, *23*, 1607–1620, doi:10.1175/2009JCLI3345.1.
- Pielke, R. A., Sr. (2002), *Mesoscale Meteorological Modeling*, Academic, San Diego, Calif.
- Pielke, R. A., Sr. (2004), Assessing “global warming” with surface heat content, *Eos Trans. AGU*, *85*, 210–211, doi:10.1029/2004EO210004.
- Radić, V., and R. Hock (2006), Modeling future glacier mass balance and volume changes using ERA-40 reanalysis and climate models: A sensi-

- tivity study at Storglaciären, Sweden, *J. Geophys. Res.*, *111*, F03003, doi:10.1029/2005JF000440.
- Reichert, B. K., L. Bengtsson, and J. Oerlemans (2001), Midlatitude forcing mechanisms for glacier mass balance investigated using general circulation models, *J. Clim.*, *14*, 3767–3784, doi:10.1175/1520-0442(2001)014<3767:MFMFGM>2.0.CO;2.
- Reijmer, C., and R. Hock (2008), Internal accumulation on Storglaciären, Sweden, in a multi-layer snow model coupled to a distributed energy- and mass-balance model, *J. Glaciol.*, *54*, 61–72, doi:10.3189/002214308784409161.
- Rotach, M. W., and D. Zardi (2007), On the boundary-layer structure over highly complex terrain: Key findings from MAP, *Q. J. R. Meteorol. Soc.*, *133*, 937–948, doi:10.1002/qj.71.
- Rotunno, R., and R. A. Houze (2007), Lessons on orographic precipitation from the Mesoscale Alpine Programme, *Q. J. R. Meteorol. Soc.*, *133*, 811–830, doi:10.1002/qj.67.
- Schneeberger, C., O. Albrecht, H. Blatter, M. Wild, and R. Hock (2001), Modelling the response of glaciers to a doubling in atmospheric CO₂: A case study of Storglaciären, northern Sweden, *Clim. Dyn.*, *17*, 825–834, doi:10.1007/s003820000147.
- Simmons, A., S. Uppala, D. Dee, and S. Kobayashi (2007), ERA-Interim: New ECMWF reanalysis products from 1989 onwards, *ECMWF Newsl.*, *110*, pp. 25–35, Eur. Cent. for Med.-Range Weather Forecasts, Reading, U. K.
- Skamarock, W. C., and J. B. Klemp (2008), A time-split nonhydrostatic atmospheric model for weather research and forecasting applications, *J. Comput. Phys.*, *227*, 3465–3485, doi:10.1016/j.jcp.2007.01.037.
- Troll, C., and K. Wien (1949), Der Lewis Gletscher am Mount Kenia, *Geogr. Ann.*, *31*, 257–274, doi:10.2307/520369.
- van den Broeke, M. R., D. van As, C. Reijmer, and R. van de Wal (2004), Assessing and improving the quality of unattended radiation observations in Antarctica, *J. Atmos. Oceanic Technol.*, *21*, 1417–1431, doi:10.1175/1520-0426(2004)021<1417:AAITQO>2.0.CO;2.
- van den Broeke, M. R., J. Bamber, J. Ettema, E. Rignot, E. Schrama, W. J. van de Berg, E. van Meijgaard, I. Velicogna, and B. Wouters (2009), Partitioning recent Greenland mass loss, *Science*, *326*, 984–986, doi:10.1126/science.1178176.
- Vizcaino, M., U. Mikolajewicz, J. Jungclaus, and G. Schurgers (2010), Climate modification by future ice sheet changes and consequences for ice sheet mass balance, *Clim. Dyn.*, *34*, 301–324, doi:10.1007/s00382-009-0591-y.
- Vuille, M., I. Juen, and G. Kaser (2008), Glacier mass balance variability in the Cordillera Blanca, Peru and its relationship with climate and the large-scale circulation, *Global Planet. Change*, *62*, 14–28, doi:10.1016/j.gloplacha.2007.11.003.
- Warner, T. T., B. E. Mapes, and M. Xu (2003), Diurnal patterns of rainfall in northwestern South America. Part II: Model simulations, *Mon. Weather Rev.*, *131*, 813–829, doi:10.1175/1520-0493(2003)131<0813:DPORIN>2.0.CO;2.
- Wastl, C., and G. Zängl (2010), Mountain-valley precipitation differences in the northern Alps: An exemplary high-resolution modeling study, *Meteorol. Atmos. Phys.*, *108*, 29–42, doi:10.1007/s00703-010-0083-y.
- Weigel, A. P., F. K. Chow, M. W. Rotach, R. L. Street, and M. Xue (2006), High-resolution large-eddy simulations of flow in a steep alpine valley. Part II: Flow structure and heat budgets, *J. Appl. Meteorol. Climatol.*, *45*, 87–107, doi:10.1175/JAM2323.1.
- Wilks, D. S. (2006), *Statistical Methods in the Atmospheric Sciences*, 2nd ed., Academic, Amsterdam.
- Winkler, M., G. Kaser, N. J. Cullen, T. Mölg, D. R. Hardy, and W. T. Pfeffer (2010), Land-based marginal ice cliffs: Focus on Kilimanjaro, *Erdkunde*, *64*, 179–193, doi:10.3112/erdkunde.2010.02.05.
- Xie, P., and P. A. Arkin (1997), Global precipitation: A 17-year monthly analysis based on gauge observations, satellite estimates, and numerical model outputs, *Bull. Am. Meteorol. Soc.*, *78*, 2539–2558, doi:10.1175/1520-0477(1997)078<2539:GPAYMA>2.0.CO;2.
- Xu, K. M., and D. A. Randall (1996), A semiempirical cloudiness parameterization for use in climate models, *J. Atmos. Sci.*, *53*, 3084–3102, doi:10.1175/1520-0469(1996)053<3084:ASCPFU>2.0.CO;2.
- Yamaguchi, S., R. Naruse, and T. Shiraiwa (2008), Climate reconstruction since the Little Ice Age by modelling Koryto glacier, Kamchatka Peninsula, Russia, *J. Glaciol.*, *54*, 125–130, doi:10.3189/002214308784409026.
- Yarnal, B. (1984), Relationships between synoptic-scale atmospheric circulation and glacier mass balance in south-western Canada during the International Hydrological Decade, 1965–74, *Ann. Glaciol.*, *30*, 188–198.
- Zängl, G., L. Gantner, G. Hartjenstein, and H. Noppel (2004), Numerical errors above steep topography: A model intercomparison, *Meteorol. Z.*, *13*, 69–76, doi:10.1127/0941-2948/2004/0013-0069.

G. Kaser and T. Mölg, Center for Climate and Cryosphere, Institute of Meteorology and Geophysics, University of Innsbruck, Innrain 52, A-6020 Innsbruck, Austria. (thomas.moelg@uibk.ac.at)